Raman studies of the intermediate tin-oxide phase

Bianca Eifert,[1] Martin Becker,[2] Christian T. Reindl,[2] Marcel Giar,[1] Lilan Zheng,[3] Angelika Polity,[2] Yunbin He,[3,*] Christian Heiliger,[1,†] and Peter J. Klar[2,‡]

[1]*Institut für Theoretische Physik, Justus-Liebig-Universität, Heinrich-Buff-Ring 16, 35392 Giessen, Germany*

[2]*I. Physikalisches Institut, Justus-Liebig-Universität, Heinrich-Buff-Ring 16, 35392 Giessen, Germany*

[3]*Hubei Collaborative Innovation Center for Advanced Organic Chemical Materials, Faculty of Materials Science and Engineering, Hubei University, Wuhan 430062, China*

(Received 1 November 2016; revised manuscript received 9 April 2017; published 26 June 2017)

The existence of an intermediate phase of tin oxide was first reported in 1882. However, its stoichiometry and its crystal structure have been dubious and heavily debated ever since, despite a multitude of structural investigations. We show that Raman spectroscopy combined with *ab initio* theory offers a viable alternative for structure determination in cases where diffraction studies are inconclusive. We unambiguously identify the intermediate phase as Sn_3O_4 and rule out the other likely candidate, Sn_2O_3. We assign the one-phonon Raman signals of Sn_3O_4 to the mode symmetries of the corresponding point group C_{2h} and confirm that $P2_1/c$ with 14 atoms per unit cell is the space group of Sn_3O_4.

DOI: 10.1103/PhysRevMaterials.1.014602

I. INTRODUCTION

Binary oxide semiconductors experience a renaissance in the light of sustainable material management. Due to their interesting properties, they are employable in a wide range of technologies. Nontoxic and earth-abundant systems of interest comprise the copper, indium, gallium, and tin oxides [1–4]. Surprisingly, some basic properties of these allegedly rather simple materials are still unknown. For example, the crystalline structures of the binary tin oxide phases are still not entirely understood, although these oxides are of considerable technological interest and known for more than a hundred years.

SnO_2 is *n* type with a direct band gap of 3.6 eV and is widely used as a transparent conducting oxide, as a gas sensor material, and as a catalyst [5]. SnO is *p* type with an indirect band gap of 0.7 eV and an optical gap of 2.7 eV [5]. The availability of a *p*- and an *n*-type semiconductor yields the potential to develop bipolar devices solely based on heterojunctions of tin oxide phases. In addition to SnO and SnO_2, an intermediate tin oxide phase is known to exist since 1882 [6]. However, despite more than a hundred years of research with x-ray diffractograms and Raman spectra published, neither its composition nor its thermodynamical stability are ultimately resolved. Conventional approaches of structure determination seem to fail. Different stoichiometries $n:m$ have been reported in literature, in particular, Sn_2O_3 [7–15] and Sn_3O_4 [16–24], both with almost the same occurrences in scientific publications. Despite its still uncertain stoichiometry, the intermediate phase is already applied to photocatalysis and shows great technological potential [25,26]. Thus, the structural analysis of this phase is now becoming more pressing than ever before.

II. PHASES OF THE TIN OXIDE SYSTEMS

As displayed in Fig. 1, SnO_2 crystallizes in the tetragonal rutile structure. SnO forms a layered tetragonal structure that can formally be derived by removing layers of oxide ions from SnO_2, similarly the intermediate monoclinic phases Sn_2O_3 and Sn_3O_4 can be constructed [19]. Additional calculations using the evolutionary algorithm of Xtalopt [27] did not yield more stable structures. Our calculated *ab initio* lattice parameters (Table I) are in excellent agreement with literature data. We used the Vienna *ab initio* simulation package (VASP) with PAW potentials [28–32]. The structural relaxation as well the calculation of the phonon frequencies and the Raman spectra have been conducted with the HSE06 hybrid functional with screened Coulomb interactions [33–35]. Usage of other functionals may lead to different lattice constants and therefore other mode frequencies.

We estimate the thermodynamical stability of the intermediate phase by constructing a phase stability diagram from *ab initio* data. The grand-canonical potential Ω of each phase serves as an indicator of its stability. It is given by $\Omega_i(\mu_O) = E_i - \mu_O N_{O,i}$, where E_i is the DFT energy of phase i, $N_{O,i}$ is the number of oxygen atoms in a cell of phase i, and μ_O is the chemical potential of oxygen in the gas phase. All cells have the same number of metal atoms, and all energies are given in reference to α-tin [38]. In Fig. 1, at any given μ_O, the tin oxide phase out of the four with the lowest Ω is most stable. Both intermediate phases are somewhat more stable than SnO and SnO_2 for a small range of oxygen potentials. It indicates that both intermediate phases are close enough to stability to be synthesizable by a nonequilibrium growth process.

The order of the intermediate phases in terms of thermal stability has to be treated cautiously. In principle more advanced methods could alter the conclusions and reverse this order. For the following discussion, it is of importance to note that the formation energies are very similar and none of the phases can be ruled out solely on the basis of these calculations, not least because the formation of the intermediate phase is likely to occur under nonequilibrium conditions and hence strictly speaking may be out of bounds of the theory.

*ybhe@hubu.edu.cn

†christian.heiliger@physik.uni-giessen.de

‡peter.j.klar@physik.uni-giessen.de

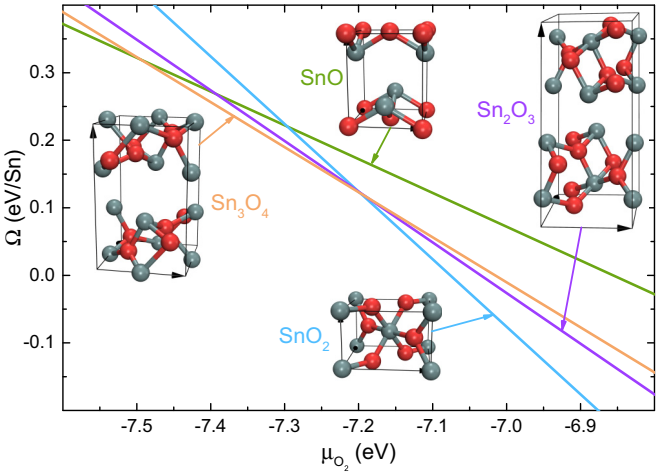

FIG. 1. Calculated stability diagram and crystal structures of the tin oxide systems. The grand-canonical potential Ω of each phase as a function of the oxygen potential μ_{O_2} serves as an indicator of its stability.

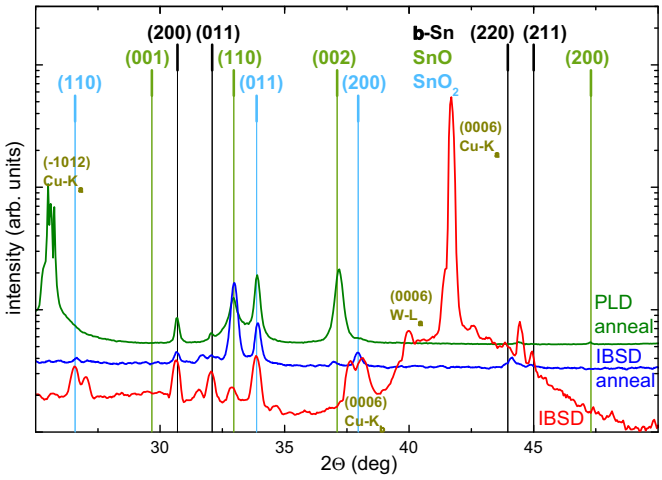

FIG. 2. XRD of the samples grown by IBSD, by IBSD followed by annealing, and by PLD followed by annealing. Prominent diffraction peaks of β-Sn, SnO and SnO_2, and sapphire substrate reflexes, i.e., (0006) for Cu-K_α, residual Cu-K_β, and W-L_α radiation and (-1012), are indicated.

III. X-RAY DIFFRACTION

We synthesized the intermediate phase by three different synthesis routes. First a film of the intermediate phase was deposited directly by ion-beam sputtering (ISBD) onto a c-sapphire substrate using the following process parameters: 5 sccm Ar flux, 4.5 sccm oxygen flux, and a substrate temperature of 550 °C [39]. Two other thin films of the intermediate phase were obtained by thermal oxidation of SnO. One SnO thin film was again deposited by IBSD on a c-sapphire substrate using 15 sccm Ar flux, 5.3 sccm O_2 flux, and a substrate temperature of 400 °C in the process.

TABLE I. Structural parameters of tin oxide phases. Experimental data obtained by XRD in this work.

Phase	Space group	Lattice parameter	This work theo	This work expt	Other
SnO	$P4/nmm$	a (Å)	3.80	3.84	3.80[a]
	(D_{4h}^7; No. 129)	c (Å)	5.02	4.83	4.84[a]
	($n = 4$)	V(Å^3)	72.6	71.2	70.0[a]
SnO_2	$P4_2/mnm$	a (Å)	4.76	4.74	4.74[b]
	(D_{4h}^{14}; No. 136)	c (Å)	3.20	3.18	3.19[b]
	($n = 6$)	V(Å^3)	72.5	71.4	71.5[b]
Sn_2O_3	$P2_1/c$	a (Å)	11.28		11.12[c]
	(C_{2h}^5, No. 14)	b (Å)	4.84		4.89[c]
	($n = 20$)	c (Å)	5.76		5.84[c]
		β (deg)	77.2		77.1[c]
		V(Å^3)	307.2		309.5[c]
Sn_3O_4	$P2_1/c$	a (Å)	8.39		8.21[c]
	(C_{2h}^5, No. 14)	b (Å)	4.89		4.93[c]
	($n = 14$)	c (Å)	5.78		5.85[c]
		β (deg)	95.0		94.7[c]
		V(Å^3)	236.0		236.0[c]

[a]Reference [36] (expt).
[b]Reference [37] (expt).
[c]Reference [19] (theo).

The subsequent oxidation took place by annealing in air for 5 h at 600 °C. Another SnO sample was grown on r-sapphire by pulsed laser deposition (PLD) from a ceramic SnO target using a laser energy of 200 mJ/pulse, a substrate temperature of 725 °C, and a deposition time of 30 min. This SnO film was converted into the intermediate phase by heating in air up to 500 °C at a rate of 50 °C/h.

The fingerprint of the crystal structure of the three samples was recorded by x-ray diffraction (XRD) in $\Theta - 2\Theta$ geometry using Cu K_α radiation (Fig. 2), the standard tool for structural characterization. Considering the constituting chemical elements, Sn and O, the deposited thin-films might comprise $\beta - Sn$, SnO, SnO_2, and intermediate phases. If we mark the prominent XRD reflexes expected in powder diffractograms of the established phases (all but the unknown intermediate phases), we find that most of the measured XRD traces already are assignable to one or more of these phases. Another complication in the XRD analysis arises from possible preferential orientations of the crystalline grains in the polycrystalline thin films. Thus, the reflex intensities of powder diffractograms need not match those of diffractograms of polycrystalline films, i.e., the assignment of the diffraction peaks becomes plurivalent. A fitting of the XRD traces also does not answer this problem, as the volume fraction of the individual phases and the preferred orientations are unknown. XRD, the standard tool for structural characterization, fails to identify the intermediate phase of tin oxide under these circumstances. It explains different structure propositions for the intermediate phase based on XRD studies in literature.

IV. RAMAN SPECTROSCOPY

Raman spectroscopy is complementary to XRD. The latter probes the static properties of the crystal structure whereas the former probes its dynamic properties. The maximum number of possible XRD reflexes is determined by the space group alone. The chemical identity of the atoms occupying the crystal

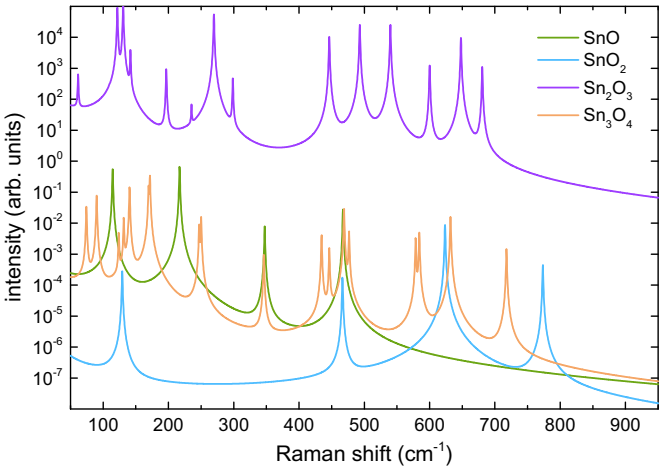

FIG. 3. Calculated Raman spectra of the different tin oxides. In the calculation a k-point mesh between $2 \times 2 \times 4$ and $8 \times 10 \times 10$ was used depending on cell size. The energy cutoff was set between 800 and 1000 eV. Our calculations of the Raman spectra followed the scheme described in Ref. [40].

sites plays a minor role in XRD, while the atomic form factors in conjunction with the symmetry of the atomic basis primarily lead to a modulation of the intensities of the XRD reflexes. In case of the lattice dynamics, i.e., the collective vibrations of the atoms about their equilibrium positions, the impact of the electronic structure is larger. For example, the Raman spectrum of a compound is strongly affected by the local bonding situation as well as by its global electronic band structure. In contrast to XRD, the number of possible Raman modes depends on the number of atoms per unit cell. The Raman tensor elements of the modes and the experimental geometry determine the mode intensities. Although the structural units of the tin oxide phases are very similar, the electronic structures differ considerably as well as the numbers of atoms per unit cell. Thus, Raman spectroscopy may be superior to XRD in identifying the intermediate tin oxide phase. However, taking full advantage of these circumstances requires an *ab initio* calculation of Raman spectra to enable a parameter-free comparison with experiment and thus to possess predictive power.

TABLE II. Point group, symmetry assignment (irrep.), and frequencies of the Raman-active modes of the tin oxide phases. The full irreducible representation is obtained as $\Gamma = \Gamma_{\mathrm{Ac}} \oplus \Gamma_{\mathrm{IR}} \oplus \Gamma_{\mathrm{R}} \oplus \Gamma_{\mathrm{Sil}}$.

symmetry of unit cell				Raman-active modes		
	point	irreducible		frequencies (cm^{-1})		
phase	group	representations	irrep.	This work (theory)	This work (experiment)	Literature
SnO	D_{4h}	$\Gamma_{\mathrm{R}} = A_{1g} \oplus B_{1g} \oplus 2E_g$	A_{1g}	217	211[a]	204[b], 211[c], 211[d]
		$\Gamma_{\mathrm{IR}} = A_{2u} \oplus E_u$	B_{1g}	347	(too weak to be detected)	350[b], 370[c]
		$\Gamma_{\mathrm{Ac}} = A_{2u} \oplus E_u$	E_{1g}	115	115[a]	107[b], 143[c], 113[d]
				467	475[a]	446[b], 494[c]
SnO_2	D_{4h}	$\Gamma_{\mathrm{R}} = A_{1g} \oplus B_{1g} \oplus B_{2g} \oplus E_g$	A_{1g}	624	639[a]	638[e], 634[f], 636[g]
		$\Gamma_{\mathrm{IR}} = A_{2u} \oplus 3E_u$	B_{1g}	129	-[×]	105[e], 123[f], 124[g]
		$\Gamma_{\mathrm{Sil}} = A_{2g} \oplus 2B_{1u}$	B_{2g}	773	-[⊗]	762[e], 776[f], 777[g]
		$\Gamma_{\mathrm{Ac}} = A_{2u} \oplus E_u$	E_g	467	480[a]	470[e], 475[f], 475[g]
Sn_2O_3	C_{2h}	$\Gamma_{\mathrm{R}} = 15A_g \oplus 15B_g$	A_g, B_g	62[†], 76[‡], 101[‡], 109[†], 122[†]		(143, 171, 238,
		$\Gamma_{\mathrm{IR}} = 14A_u \oplus 13B_u$		131[†], 142[†], 147[‡], 155[‡], 190[‡]		245, 341,433,
		$\Gamma_{\mathrm{Ac}} = A_u \oplus 2B_u$		197[†], 235[†], 246[‡], 270[†], 278[‡]		450, 472,584,
				299[†], 304[‡], 371[‡], 446[†], 452[‡],		633, 691, 775)[h*]
				493[†], 494[‡], 537[‡], 540[†], 580[‡]		
				600[†], 648[†], 681[†], 687[‡], 742[‡]		(110, 134, 143,
Sn_3O_4	C_{2h}	$\Gamma_{\mathrm{R}} = 9A_g \oplus 9B_g$	A_g, B_g	74[†], 90[‡], 124[†], 132[‡], 140[†]	73, 90, 130, 140	172, 212, 239,
		$\Gamma_{\mathrm{IR}} = 11A_u \oplus 10B_u$		170[‡], 172[†], 247[†], 250[‡], 346[‡]	170, 238, 244, 338	247, 433, 447,
		$\Gamma_{\mathrm{Ac}} = A_u \oplus 2B_u$		435[†], 446[‡], 469[‡], 477[†], 579[‡]	433, 448, 472, 480	473, 540, 586,
				584[†], 632[†], 718[‡]	579, 588, 627, 700	632,695, 776)[i*]

[a]Reference [39] (own previous work).
[b]Reference [41] (theo).
[c]Reference [42] (theo).
[d]Reference [43] (expt).
[e]Reference [44] (theo).
[f]Reference [45] (expt).
[g]Reference [46] (expt).
[†]A_g-mode.
[‡]B_g-mode.
[h]Reference [47] (expt).
[i]Reference [48] (expt).
[*]unclear stoichiometry and crystal structure.
[×]not detectable with the setup used in Ref. [39].
[⊗]not detectable because of overlap with modes of sapphire substrate.

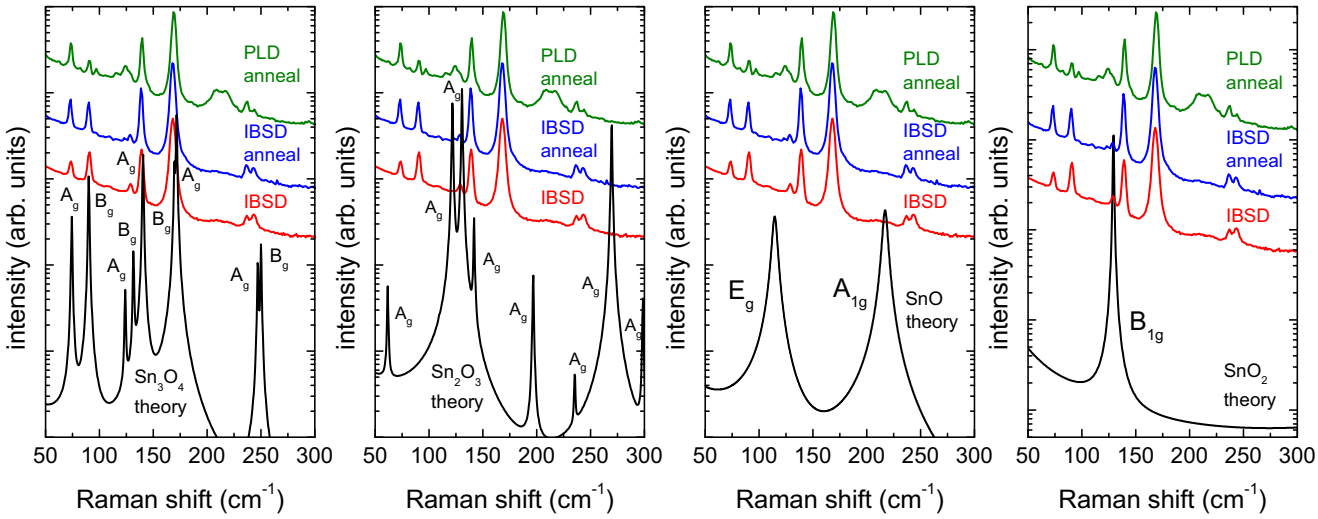

FIG. 4. Experimental Raman spectra of the three samples of the intermediate phase compared to the theoretical spectra of Sn_3O_4, Sn_2O_3, SnO, and SnO_2 (left to right). Only the spectrum calculated for Sn_3O_4 matches the experimental data.

To highlight the strength of Raman spectroscopy, we calculated the first-order Raman spectra of the four tin oxide phases shown in Fig. 3 by an *ab initio* approach. Table II gives frequencies and symmetry assignment of the corresponding modes. The spectra differ considerably in the number of Raman signals (reflecting the different numbers of basis atoms) and in the frequencies of the modes (reflecting the force constants arising from the differences in bonding). The scattering cross sections of one-phonon Raman processes depend on the electronic band structure of the compound, in particular, on changes of the polarizability induced by the vibrational modes. Sn_2O_3 turns out to be the strongest Raman scatterer, followed by SnO and Sn_3O_4, and finally SnO_2 as the weakest Raman scatterer among the four compounds. Two main conclusions can be drawn from the theoretical spectra of Fig. 3. First, even traces of Sn_2O_3 present in other tin oxide phases should be observable by Raman spectroscopy. Second, the main differences in the Raman spectra of the four compounds are below a Raman shift of about 300 cm^{-1}. This finding together with the fact that theory does not account for higher-order Raman scattering processes leads us to focus on low Raman shifts in the comparison between theory and experiment.

Figure 4 consists of four graphs each depicting the Raman spectra of the three thin-film samples of the intermediate phase in comparison with theoretical Raman spectra of the four considered tin oxide phases. Raman spectra were acquired at 22 °C using a Renishaw inVia Raman microscope system with an excitation wavelength of 633 nm. The spectral range is 50 to 300 cm^{-1}. The differences between the experimental spectra of the three samples obtained by the different synthesis routes, i.e., additional features at about 120 cm^{-1} and 213 cm^{-1} in the case of the PLD sample, can be explained by traces of SnO in the PLD grown film. This finding underlines again the difficulty to stabilize the intermediate oxide phase.

The two theoretical Raman spectra in the two graphs on the left of Fig. 4 allow us to clearly distinguish between the two candidate structures. The theoretical spectrum derived for the proposed Sn_3O_4 structure reproduces the four main features assigned to the intermediate phase in peak positions as well as in signal strength. It also satisfactorily reproduces the feebler features of the spectrum between 120 and 140 cm^{-1} and at about 250 cm^{-1}. In contrast, the theoretical Raman spectrum of the proposed Sn_2O_3 structure cannot reproduce the four main features of the experimental Raman spectra of the intermediate phase at all and predicts its strongest Raman features at Raman shifts where no modes occur in experiment. Keeping in mind that Sn_2O_3 is a very strong Raman scatterer according to our *ab initio* results shown in Fig. 3, we can rule out any trace of this phase in our thin-film samples. On the basis of this analysis, we can unambiguously assign the stoichiometry and crystal structure of the intermediate phase to monoclinic Sn_3O_4.

The definite knowledge of the Sn_3O_4 structure and its point group C_{2h} now yields the irreducible representations of the optical vibrational modes at the zone center $\Gamma = 9A_g \oplus 9B_g \oplus 11A_u \oplus 10B_u$, of which only the A_g and B_g are Raman active yielding in total 18 Raman active modes. Our calculated mode frequencies of the Raman-active modes agree well with experiment as shown in Fig. 4 and listed in Table II. The Raman tensors of the A_g and B_g modes are given by:

$$\mathcal{R}(A_g) = \begin{pmatrix} a & 0 & d \\ 0 & b & 0 \\ d & 0 & c \end{pmatrix} \quad \mathcal{R}(B_g) = \begin{pmatrix} 0 & e & 0 \\ e & 0 & f \\ 0 & f & 0 \end{pmatrix}. \quad (1)$$

As only a few elements of both tensors are zero, it is very likely that all Raman-allowed modes will appear in the spectra of somewhat polycrystalline samples when no polarization optics are used for detection. This explains not only why all Raman-active modes are indeed observed in our experiments but also why the Raman spectra reported here agree well in frequencies and also peak intensities with those in literature. Unfortunately a verification of the mode assignment by polarization-dependent experiments is very difficult, as the degree of polycrystallinity of the films, i.e., whether the orientations of the crystalline grains are fully at random or a preferential orientation exists, is unknown. Thus, Raman selection rules are difficult to employ as the scattering geometry is ill defined.

V. CONCLUSIONS

In conclusion, Raman spectroscopy in conjunction with *ab initio* theory is a powerful tool for identifying crystal structures in cases where commonly used standard diffraction methods alone cannot give a decisive answer. The inverse problem of deducing a crystal structure from its Raman spectrum is unsolvable, as is the equivalent problem for an XRD trace. In both cases, the identification of the corresponding crystal structure must rely on calculating spectra or traces of likely candidate structures and comparing them with experiment. The Raman approach, though more cumbersome, can be advantageous compared to standard XRD, in particular in some cases where candidate structures possess a large number of atoms per unit cell. As a particular example, we unravelled the long-standing mystery of the intermediate phase of the tin oxide material system and assigned this phase unambiguously to monoclinic Sn_3O_4. Our analysis is based on Sn_3O_4 thin films prepared by three different approaches. Furthermore, Raman spectra reported in literature for nanostructures of the intermediate tin oxide phase are in accordance with our spectra [8,49]. We believe that it is very likely that Sn_3O_4 is obtained as intermediate phase independent of the synthesis process and that previous reports of observed Sn_2O_3 might be faulty due to the difficulties to distinguish the monoclinic structures of Sn_2O_3 and Sn_3O_4 by standard diffraction analysis.

ACKNOWLEDGMENTS

We thank the late Bruno K. Meyer for numerous productive discussions. Y.H. acknowledges the financial support from National Natural Science Foundation of China (Grants No. 61274010 and No. 51572073).

[1] E. Fortunato, P. Barquinha, and R. Martins, Adv. Mater. **24**, 2945 (2012).
[2] G. Eranna, B. C. Joshi, D. P. Runthala, and R. P. Gupta, Crit. Rev. Solid State Mater. Sci. **29**, 111 (2004).
[3] K. Ellmer, Nat. Photon. **6**, 809 (2012).
[4] B. K. Meyer, A. Polity, D. Reppin, M. Becker, P. Hering, P. J. Klar, T. Sander, C. Reindl, J. Benz, M. Eickhoff, C. Heiliger, M. Heinemann, J. Bläsing, A. Krost, S. Shokovets, C. Müller, and C. Ronning, Phys. Status Solidi B **249**, 1487 (2012).
[5] M. Batzill and U. Diebold, Prog. Surf. Sci. **79**, 47 (2005).
[6] M. A. Ditte, Ann. Chim. Phys. **27**, 147 (1882).
[7] G. Murken and M. Trömel, Z. Anorg. Allg. Chem. **397**, 117 (1973).
[8] L. Sangaletti, L. E. Depero, B. Allieri, F. Pioselli, E. Comini, G. Sberveglieri, and M. Zocchi, J. Mater. Res. **13**, 2457 (1998).
[9] M. S. Moreno, R. F. Egerton, and P. A. Midgley, Phys. Rev. B **69**, 233304 (2004).
[10] A. Martel, F. Caballero-Briones, P. Bartolo-Perez, A. Iribarren, R. Castro-Rodriguez, A. Zapata-Navarro, and J. Pena, Surf. Coat. Technol. **148**, 103 (2001).
[11] W. K. Choi, H. Sung, K. H. Kim, J. S. Cho, S. C. Choi, H.-J. Jung, and S. K. Koh, J. Mater. Sci. Lett. **16**, 1551 (1997).
[12] H. Giefers, F. Porsch, and G. Wortmann, Solid State Ionics **176**, 199 (2005).
[13] M. S. Moreno, R. C. Mercader, and A. G. Bibiloni, J. Phys.: Condens. Matter **4**, 351 (1992).
[14] J. Geurts, S. Rau, W. Richter, and F. Schmitte, Thin Solid Films **121**, 217 (1984).
[15] M. A. Mäki-Jaskari and T. T. Rantala, Modell. Simul. Mater. Sci. Eng. **12**, 33 (2004).
[16] F. Lawson, Nature (London) **215**, 955 (1967).
[17] T. A. White, M. S. Moreno, and P. A. Midgley, Z. Kristallogr. **225**, 56 (2010).
[18] Z. R. Dai, Z. W. Pan, and Z. L. Wang, J. Am. Chem. Soc. **124**, 8673 (2002).
[19] X. Lu, S. G. J. Mochrie, S. Narayanan, A. R. Sandy, and M. Sprung, Phys. Rev. Lett. **100**, 045701 (2008).
[20] L.-Z. Yang, Z.-T. Sui, and C.-Z. Wang, J. Solid State Chem. **113**, 221 (1994).
[21] F. Gauzzi, B. Verdini, A. Maddalena, and G. Principi, Inorganica Chimica Acta **104**, 1 (1985).
[22] X. Q. Pan and L. Fu, J. Appl. Phys. **89**, 6048 (2001).
[23] S. Cahen, N. David, J. Fiorani, A. Maitre, and M. Vilasi, Thermochim. Acta **403**, 275 (2003).
[24] M. S. Moreno, G. Punte, G. Rigotti, R. C. Mercader, A. D. Weisz, and M. A. Blesa, Solid State Ionics **144**, 81 (2001).
[25] Y. He, D. Li, J. Chen, Y. Shao, J. Xian, X. Zheng, and P. Wang, RSC Advances **4**, 1266 (2014).
[26] M. Manikandan, T. Tanabe, P. Li, S. Ueda, G. V. Ramesh, R. Kodiyath, J. Wang, T. Hara, A. Dakshanamoorthy, S. Ishihara, K. Ariga, J. Ye, N. Umezawa, and H. Abe, Appl. Mater. Interfaces **6**, 3790 (2014).
[27] D. C. Lonie and E. Zurek, Comput. Phys. Commun. **182**, 372 (2011).
[28] G. Kresse and J. Hafner, Phys. Rev. B **47**, 558 (1993).
[29] G. Kresse and J. Hafner, Phys. Rev. B **49**, 14251 (1994).
[30] G. Kresse and J. Furthmüller, Comput. Mat. Sci. **6**, 15 (1996).
[31] G. Kresse and J. Furthmüller, Phys. Rev. B **54**, 11169 (1996).
[32] G. Kresse and D. Joubert, Phys. Rev. B **59**, 1758 (1999).
[33] J. Heyd, G. E. Scuseria, and M. Ernzerhof, J. Chem. Phys. **118**, 8207 (2003).
[34] J. Heyd, G. E. Scuseria, and M. Ernzerhof, J. Chem. Phys. **124**, 219906 (2006).
[35] J. Heyd and G. E. Scuseria, J. Chem. Phys. **121**, 1187 (2004).
[36] J. Pannetier and G. Denes, Acta Cryst. **B36**, 2763 (1980).
[37] W. Baur, Acta Cryst. **9**, 515 (1956).
[38] D. S. Sholl and J. A. Steckel, *Density Functional Theory* (Wiley, Hoboken, New Jersey, 2009).
[39] M. Becker, A. Polity, and P. J. Klar, Phys. Status Solidi RRL **9**, 326 (2015).
[40] P. Umari, A. Pasquarello, and A. Dal Corso, Phys. Rev. B **63**, 094305 (2001).
[41] Y. W. Li, Y. Li, T. Cui, L. J. Zhang, Y. M. Ma, and G. T. Zou, J. Phys.: Condens. Matter **19**, 425230 (2007).
[42] E. L. Peltzery Blanca, A. Svane, N. E. Christensen, C. O. Rodriguez, O. M. Cappannini, and M. S. Moreno, Phys. Rev. B **48**, 15712 (1993).
[43] X. Wang, F. X. Zhang, I. Loa, K. Syassen, M. Hanfland, and Y.-L. Mathis, Phys. Stat. Sol. B **241**, 3168 (2004).

[44] K. Parlinski and Y. Kawazoe, Eur. Phys. J. B **13**, 679 (2000).
[45] P. S. Peercy and B. Morosin, Phys. Rev. B **7**, 2779 (1973).
[46] H. Hellwig, A. F. Goncharov, E. Gregoryanz, H.-k. Mao, and R. J. Hemley, Phys. Rev. B **67**, 174110 (2003).
[47] F. Wang, X. Zhou, J. Zhou, T.-K. Sham, and Z. Ding, J. Phys. Chem. C **111**, 18839 (2007).
[48] O. M. Berengue, R. A. Simon, A. J. Chiquito, C. J. Dalmaschio, E. R. Leite, H. A. Guerreiro, and F. E. G. Guimaraes, J. Appl. Phys. **107**, 033717 (2010).
[49] C. J. Damaschio, O. M. Berengue, D. G. Stroppa, R. A. Simon, A. J. Ramirez, W. H. Schreiner, A. J. Chiquito, and E. R. Leite, J. Cryst. Growth **312**, 2881 (2010).